

Merging Cation Exchange and Photocatalytic Charge Separation Efficiency in an Anatase/ $K_2Ti_4O_9$ Nanobelt Heterostructure for Metal Ions Fixation

Yusuke Ide,^{*,†} Wataru Shirae,[‡] Toshiaki Takei,[†] Durai Mani,^{†,§} and Joel Henzie[†]

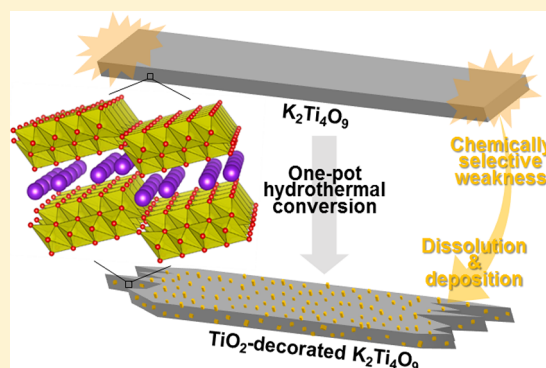
[†]International Center for Materials Nanoarchitectonics (MANA), National Institute for Materials Science (NIMS), 1-1 Namiki Tsukuba, Ibaraki 305-0044, Japan

[‡]Graduate School of Creative Science and Engineering, Waseda University, 1-6-1 Nishiwaseda, Shinjuku-ku, Tokyo 169-8050, Japan

[§]Center for Nanoscience and Technology, Anna University, Chennai 600025, India

Supporting Information

ABSTRACT: Efficient collection and safe disposal of toxic metal ions from aqueous solutions is critical for applications in environmental remediation. Although extensive efforts have been devoted to the synthesis of functional TiO_2 materials, photocatalytic reduction (photoreduction) of aqueous metal ions into solid metals remains a challenge. We designed a TiO_2 nanoparticle-decorated layered titanate ($K_2Ti_4O_9$) material that retained the cation exchange ability of $K_2Ti_4O_9$, but also possessed the enhanced charge separation efficiency of $K_2Ti_4O_9$. Combining cation exchange with enhanced charge separation efficiency results in a heterostructured material with remarkably high activity for the photoreduction of metal ions. Initially we demonstrated how the photocatalyst can efficiently reduce aqueous Ni^{2+} cations, whereas the benchmark TiO_2 -based P25 catalyst showed little to no activity. The resulting Ni-deposited heterostructure can then be used as a catalyst for visible light-induced photocatalytic H_2 evolution in water.



INTRODUCTION

Using light to reduce metal ions in water and deposit them on solid surfaces is a topic covering a wide range of scientific and practical purposes, with applications spanning the removal of toxic ions to the collection of useful metals. Photocatalytic collection of ions is a safer disposal process than most adsorption and ion exchange processes because the adsorbed metal ions can be spontaneously reduced to fix metals on surfaces.¹ There are many kinds of photocatalysts, but TiO_2 is one of the most stable and cost-effective materials. However, despite great progresses on advanced TiO_2 synthesis methods, the photocatalytic reduction of metal ions (e.g., Ni^{2+} and Cd^{2+}) is still challenging, in part because TiO_2 has poor adsorption affinity for metal ions, which is necessary for photoreduction to occur.^{2–6}

Layered inorganic solids including layered clay minerals have historically been used as ion exchange materials owing to their large surface areas and large adsorption capacities. Their high capacities stem from the structure of the material; layered materials composed of nanometer-thick nanosheets have better chemical and thermal stabilities than their organic counterparts.^{7,8} For example, layered titanates are composed of titania nanosheets separated by interlayers of alkali metal cations and are known to be excellent ion exchange materials.^{9–12} Although layered titanates have been widely investigated as photo-

catalysts,^{13–19} they exhibit poor photocatalytic activity without any modification.^{20,21} Typically, titanate nanosheets are modified by exfoliating them in the presence of other functional materials.^{14–19} This process hybridizes the two materials, but frequently causes the titanate to lose its original ion exchange ability. In the pursuit of higher photocatalytic activity, most existing work in the literature does not address the loss of ion exchange ability, or attempt to discover ways to mitigate loss. We hypothesized that layered titanate-based hybrid photocatalysts that maintained their original cation exchange properties will possess extraordinary performance for the photocatalytic reduction of metal ions if they were properly synthesized.

Herein, we report on design of a TiO_2 (anatase)-modified layered titanate ($K_2Ti_4O_9$) photocatalyst via a simple one-pot hydrothermal reaction. This photocatalyst has remarkably high performance for the photoreduction of Ni^{2+} cations from water, whereas P25-type TiO_2 is inactive. Ni was chosen as the target aqueous cation because it is a common water contaminant that occurs in high concentrations in the environment, and is also a valuable metal in various technologies.^{22,23}

Received: March 1, 2018

The present hydrothermal reaction for TiO₂-based materials builds on a method previously developed by our group.^{24–26} For example, amorphous TiO₂ is chemically less resistant to etching agents than crystalline phases. P25-type TiO₂ is mainly composed of anatase and rutile TiO₂ and contains some fraction of amorphous TiO₂, which we exploit by dissolving it and then recrystallizing on the main crystals under hydrothermal conditions. The new crystallites are anatase and rutile phases, and the new heterostructure system behaves as a high-performance photocatalyst.²⁴ In this study, K₂Ti₄O₉ nanobelts were exposed to similar hydrothermal conditions. To our surprise, the edges of the nanobelts selectively dissolved and recrystallized into anatase nanoparticles, forming heterostructure photocatalysts that retain the cation exchange ability of the original titanate (Figure 1).

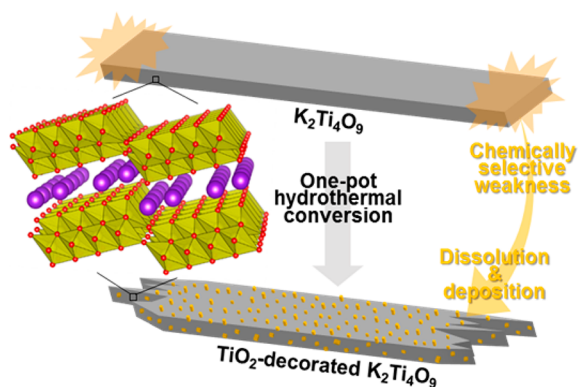


Figure 1. Scheme for design of anatase-modified layered titanate (K₂Ti₄O₉) having the original cation exchange ability.

RESULTS AND DISCUSSION

K₂Ti₄O₉ nanobelts were prepared by a solid state reaction between K₂CO₃ and TiO₂ (anatase) according to the literature.²⁷ We hydrothermally treated K₂Ti₄O₉ under alkali conditions in the presence of tetrapropylammonium hydroxide (TPA) and ammonium fluoride (NH₄F). According to our previous experiments, both reagents should promote the dissolution of K₂Ti₄O₉, while NH₄F acted as mineralizer to recrystallize the dissolved species.^{24–26} We named the hydrothermal product Hyd-K₂Ti₄O₉. XRD analysis (Figure 2, left a and b) revealed that the hydrothermal reaction caused the

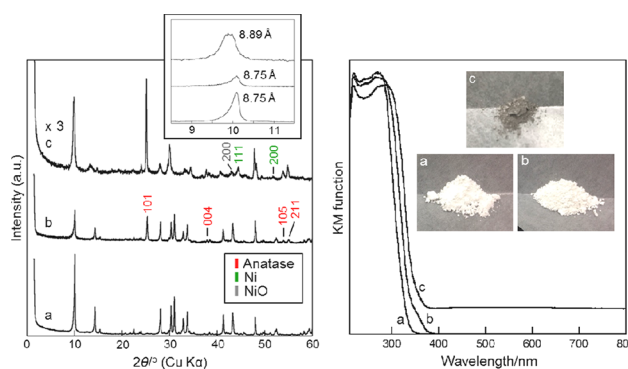


Figure 2. (left) XRD patterns and (right) UV-vis spectra of (a) K₂Ti₄O₉, (b) Hyd-K₂Ti₄O₉, and (c) Hyd-K₂Ti₄O₉ after the photocatalytic Ni²⁺ reduction. Insets show the expanded figure at low 2θ region and the photographs of each sample.

peaks assigned to K₂Ti₄O₉ to weaken, while new XRD peaks matching anatase appeared. The basal spacing of Hyd-K₂Ti₄O₉, 0.88 nm, was identical to K₂Ti₄O₉, suggesting that no intercalation reaction occurred during the hydrothermal reaction. UV-vis spectroscopy of the Hyd-K₂Ti₄O₉ sample also confirmed the presence of anatase, which has a narrower band gap (i.e., longer-wavelength absorption edge) than K₂Ti₄O₉ (Figure 2, right).^{17–19}

Figure 3a,b shows SEM images of K₂Ti₄O₉ and Hyd-K₂Ti₄O₉. The K₂Ti₄O₉ nanobelt-shaped particles had thicknesses of up to a few hundreds of nanometers and lengths of up to several microns. The Hyd-K₂Ti₄O₉ sample was also shaped like a nanobelt. However, high-magnification SEM micrographs for Hyd-K₂Ti₄O₉ (Figure 3c) revealed the presence of tiny particles covering the surface of each nanobelt. HRTEM (Figure 3d) showed that these smaller particles (ca. 10–30 nm) were anatase, consistent with the XRD and UV data (Figure 2). Both phases are bonded together by a particle interface according to HRTEM, selected area electron diffraction (SAED), high-angle annular dark field scanning TEM (HAADF-STEM), and energy-dispersive X-ray spectroscopy (EDX) measurements shown in Figure S1. In sum, these results prove that Hyd-K₂Ti₄O₉ is a heterostructure material composed of K₂Ti₄O₉ nanobelts decorated with anatase nanoparticles.

Interestingly, SEM (Figure 3b) and TEM and HRTEM (Figure 3e,f) observations showed that many Hyd-K₂Ti₄O₉ nanobelts had uneven edges that extended into nanowires, whereas the original K₂Ti₄O₉ nanobelts had relatively smooth edges. Since the thickness and length of K₂Ti₄O₉ nanobelts scarcely changed after the hydrothermal reaction, the edges of K₂Ti₄O₉ nanobelts were selectively dissolved and recrystallized into anatase to form Hyd-K₂Ti₄O₉ during the hydrothermal reaction. It is well-known that K₂Ti₄O₉ can be exfoliated into nanosheets without significant change in the lateral size of the layers in alkali solutions containing tetrabutylammonium hydroxide.^{17–19} In contrast, P25-type TiO₂ (composed of anatase, rutile, and amorphous phases) treated under the similar hydrothermal conditions causes the amorphous phase to selectively dissolve and convert into new anatase and rutile crystals in an uncontrolled manner.²⁴ Dissolution in layered K₂Ti₄O₉ titanate nanobelts happens primarily at the edges, which can be dissolved more easily. This is the first report on the intraparticle regioselective chemical weakness of layered titanates.

More importantly, after the hydrothermal reaction, the cation exchange ability of K₂Ti₄O₉ was retained. We examined the adsorption of Ni²⁺ on different materials from water containing NiCl₂ and methanol (pH = 4.7), which was the same solution used in photocatalytic Ni²⁺ deposition experiments described in detail below. As shown in Figure 4a, K₂Ti₄O₉ effectively adsorbed Ni²⁺ with a maximum adsorption amount of >1 mmol g⁻¹, which was almost identical to the cation exchange capacity (1.2 mmol g⁻¹ for divalent cations at this pH region).¹⁰ This result shows that cation exchange of interlayer K⁺ and replacement with Ni²⁺ is almost complete. We compared the Ni²⁺ adsorption of TiO₂ (P25) and found it was negligible, consistent with previous reports.²⁴ This is understandable because the surface of P25 is positively charged below the isoelectric point (ca. 6.4)²⁸ and repels cations. On the other hand, Hyd-K₂Ti₄O₉ had a cation exchange ability comparable to that of K₂Ti₄O₉. The slight decrease in the maximum amount of the adsorbed cation can be explained by the fact that a part of the K₂Ti₄O₉ surface was converted into anatase.

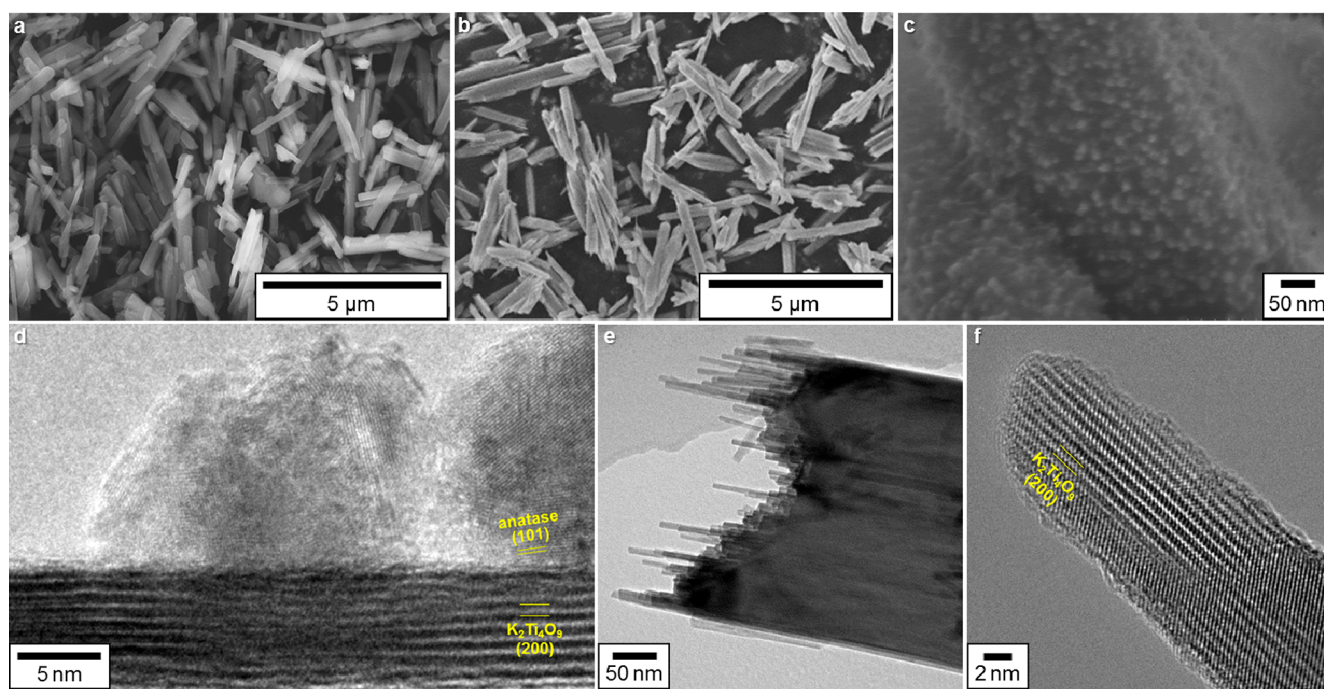


Figure 3. SEM images of (a) $\text{K}_2\text{Ti}_4\text{O}_9$ and (b) $\text{Hyd-K}_2\text{Ti}_4\text{O}_9$. (c) High-magnification SEM and (d) HRTEM images of $\text{Hyd-K}_2\text{Ti}_4\text{O}_9$, (e) TEM and (f) HRTEM images of the edge of $\text{Hyd-K}_2\text{Ti}_4\text{O}_9$, showing the presence of $\text{K}_2\text{Ti}_4\text{O}_9$ nanowires.

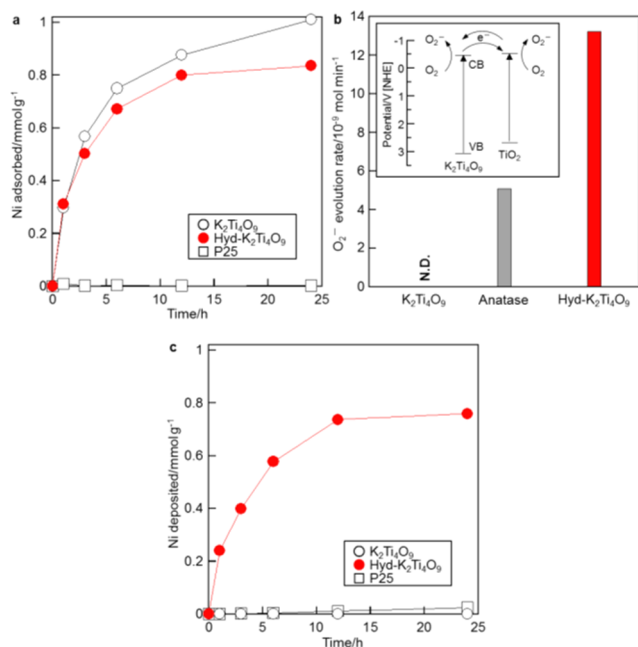


Figure 4. (a) Ni^{2+} adsorption rates from water containing methanol on P25, $\text{K}_2\text{Ti}_4\text{O}_9$, and $\text{Hyd-K}_2\text{Ti}_4\text{O}_9$. (b) O_2^- evolution rates on $\text{K}_2\text{Ti}_4\text{O}_9$, anatase, $\text{Hyd-K}_2\text{Ti}_4\text{O}_9$. Inset shows energy diagram and scheme for electron transfer between anatase and $\text{K}_2\text{Ti}_4\text{O}_9$ components in $\text{Hyd-K}_2\text{Ti}_4\text{O}_9$ under light irradiation. (c) Ni^{2+} deposition rates from water containing methanol on P25, $\text{K}_2\text{Ti}_4\text{O}_9$, and $\text{Hyd-K}_2\text{Ti}_4\text{O}_9$ under light irradiation.

In addition to the cation exchange ability, the enhanced charge separation efficiency of $\text{Hyd-K}_2\text{Ti}_4\text{O}_9$ was examined to determine if it could catalyze the photoreduction of metals. The O_2^- yield from TiO_2 was quantitatively monitored using nitroblue tetrazolium (NBT). NBT reacts with O_2^- generated by a reaction between O_2 and photoexcited electrons of the

TiO_2 -based photocatalyst. This reaction causes the NBT to convert into insoluble Formazan that deposited on the surface of TiO_2 .^{20,29} $\text{K}_2\text{Ti}_4\text{O}_9$ did not generate any O_2^- according to the NBT assay (Figure 4b), whereas $\text{Hyd-K}_2\text{Ti}_4\text{O}_9$ generated a considerably higher amount of O_2^- than our JRC TIO-1 anatase benchmark sample, even though the anatase component in $\text{Hyd-K}_2\text{Ti}_4\text{O}_9$ and the JRC TIO-1 were similar in size (the JRC TIO-1 was supplied by Catalysis Society of Japan). Considering the fact that the conduction band potential (E_{CB}) of $\text{K}_2\text{Ti}_4\text{O}_9$ is almost identical to that of anatase,^{17–19} electron transfer from photoexcited $\text{K}_2\text{Ti}_4\text{O}_9$ to anatase and vice versa is thermodynamically favorable, and both components can synergistically enhance the charge separation of the combined system (Figure 4b, inset).

As expected, $\text{Hyd-K}_2\text{Ti}_4\text{O}_9$ showed a remarkably high activity for the photoreduction of Ni^{2+} in water to Ni under irradiation with a solar simulator. The photoreduction tests were conducted using methanol as a sacrificial reagent. TiO_2 (and $\text{K}_2\text{Ti}_4\text{O}_9$) cannot directly reduce Ni^{2+} because its E_{CB} is lower (more positive) than the reduction potential of the Ni^{2+}/Ni couple at ambient pH (pH < 7). However, TiO_2 -based materials can indirectly reduce Ni^{2+} cations with radical reductant species formed by the oxidation of an organic additive (e.g., methanol) via the TiO_2 -photogenerated holes.^{2–5} As shown in Figure 4c, P25 reduced/deposited only a tiny amount of Ni^{2+} into Ni metal, consistent with previous reports.^{2–6} Pure $\text{K}_2\text{Ti}_4\text{O}_9$ showed no proficiency for this reaction. In contrast, $\text{Hyd-K}_2\text{Ti}_4\text{O}_9$ efficiently reduced Ni^{2+} to Ni under the identical irradiation conditions. The Ni deposition was also confirmed by XRD and UV–vis analysis (Figure 2c): the gray color of the product indicates the deposited Ni is partially oxidized. We called the present reduction reaction “photoinduced reduction” hereafter because the structure of $\text{Hyd-K}_2\text{Ti}_4\text{O}_9$ changed after the reaction.

The location of the Ni metal in the recovered product was used to clarify part of the mechanism for photoinduced Ni^{2+}

deposition by Hyd-K₂Ti₄O₉. The cross-sectional HRTEM and HADDF-STEM images of the Ni-deposited Hyd-K₂Ti₄O₉ (Figure 5) reveal that Ni (or NiO) was deposited inside the

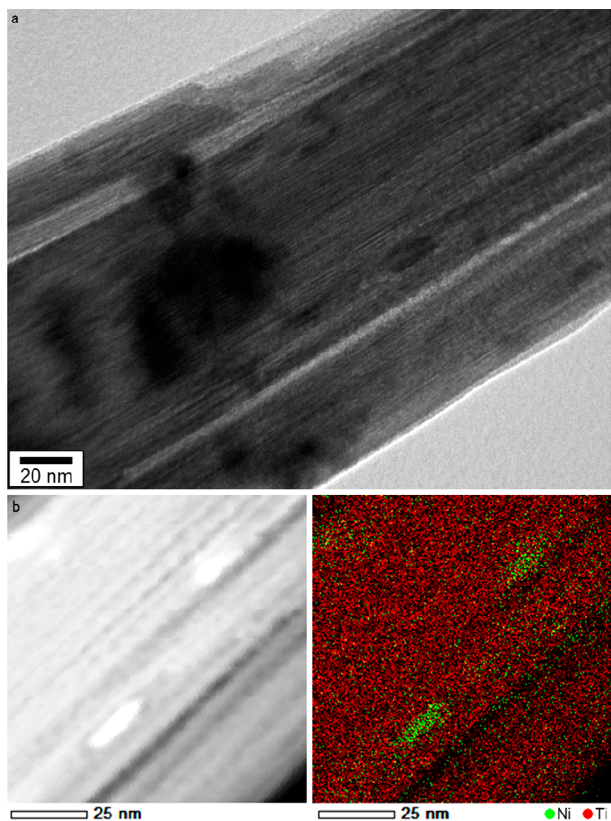


Figure 5. Cross-sectional (a) HRTEM image and (b) HADDF-STEM image and the corresponding EDX elemental map of Hyd-K₂Ti₄O₉ after photocatalytic Ni deposition.

titanate particles, rather than on the outer surface of the particle (additional STEM images are shown in Figure S2, together with their corresponding EDX elemental maps and EDX spectra). Additionally, many of the Ni particles had a plate-like shape, strongly suggesting that the two-dimensional interlayer nanospace served as a template during the growth of the Ni nanoparticle.^{30,31} Considering that the XRD peak due to the basal spacing was shifted to the lower 2θ region and substantially broadened after the Ni deposition (Figure 2c), we concluded that Hyd-K₂Ti₄O₉ effectively concentrates Ni²⁺ from water into the interlayer space and reduces it there in the presence of methanol and the assistance of photoirradiation.

The HADDF-STEM of Ni-deposited Hyd-K₂Ti₄O₉ also showed that a part of Ni (or NiO) particles was deposited on the external surface (Figure S3). In the XPS spectrum (Figure S4), Ni-deposited Hyd-K₂Ti₄O₉ had a peak at 856 eV, which is assigned to NiO interacting with supports including TiO₂.^{32,33} From XRD, HRTEM/HADDF-STEM, and XPS data described above, we can conclude that Ni deposited on the surface of the particle was oxidized to NiO, while the Ni deposited inside the particle remained metallic. We cannot, however, rule out the possibility that the presence of both Ni and NiO results from difference in reactivity toward O₂ between anatase and K₂Ti₄O₉.

To gain a deeper insight into the mechanism, the ability of the photocatalyst to drive methanol oxidation and methanol

adsorption was examined in detail. Figure 6a shows the photocatalytic activity of different materials for the complete

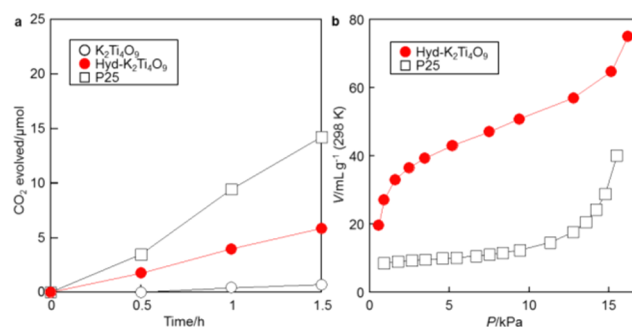


Figure 6. (a) CO₂ evolution rates from methanol in water on P25, K₂Ti₄O₉, and Hyd-K₂Ti₄O₉ under light irradiation. (b) Adsorption isotherms of methanol on P25 and Hyd-K₂Ti₄O₉.

oxidation of methanol into CO₂ in water. Hyd-K₂Ti₄O₉ had considerably enhanced activity compared with the starting material K₂Ti₄O₉. This confirms the O₂⁻ evolution data (Figure 4b) and strongly suggests the formation of methanol-derived radical species, capable of reducing Ni²⁺ to Ni during the photoirradiation. The CO₂ evolution rate on Hyd-K₂Ti₄O₉ was moderate compared to P25, a benchmark TiO₂ for oxidation of organic compounds.^{34,35} It is likely that the moderate methanol oxidation activity of Hyd-K₂Ti₄O₉ is afforded by the longer lifetime of the radical species. On the other hand, Hyd-K₂Ti₄O₉ adsorbed methanol more strongly and had a higher capacity than P25 according to the adsorption isotherm (Figure 6b). These results confirmed the above scenario.

The results presented above indicate that Hyd-K₂Ti₄O₉ can be used for the efficient removal and safe disposal of metal ions, which cannot be achieved by conventional TiO₂ photocatalytic systems. Since Ni²⁺ ions and NiO clusters are known to sensitize TiO₂ photocatalysts,^{36–38} we tested the resulting Ni-deposited Hyd-K₂Ti₄O₉ materials for visible light-induced photocatalytic H₂ evolution via water splitting. As shown in Figure 7, the Ni@Hyd-K₂Ti₄O₉ material exhibited enhanced

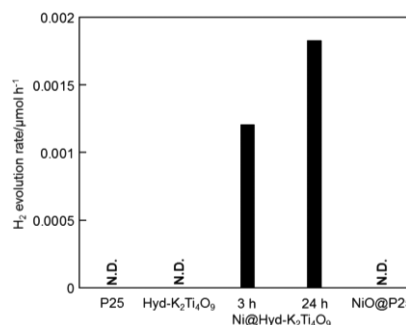


Figure 7. Rate of H₂ evolution from water containing methanol from P25, Hyd-K₂Ti₄O₉, Ni@Hyd-K₂Ti₄O₉ (3 h and 24 h irradiation products in Figure 4c) and NiO@P25 (Ni loading of 0.5 wt %) under photoirradiation.

activity at visible wavelengths ($\lambda > 450$ nm) because it is a strong light absorber in this region (Figure 2, right). The apparent quantum yield at 450 nm was 0.0002%. In contrast, P25 and Hyd-K₂Ti₄O₉ did not show activity under identical irradiation conditions because their absorption cross section is almost zero at $\lambda > 450$ nm.

As a reference, we prepared NiO cluster-grafted TiO₂ (NiO@P25) showing $\lambda > 450$ nm light absorption (Figure S5) via chemisorption of nickel(II) acetylacetonate, followed by calcination.^{36,37} The NiO@P25 was not photocatalytically active under identical conditions. This result suggests the important role of the Ni species present in the Ni@Hyd-K₂Ti₄O₉ material, including plate-like Ni nanoparticles which may enhance activity.

CONCLUSION

We reported a simple hydrothermal method to selectively dissolve the edges of layered titanate (K₂Ti₄O₉) nanobelts. Anatase nanocrystals recrystallize on the K₂Ti₄O₉ surfaces, forming heterostructures that exhibit (i) superb cation exchange ability comparable to the titanate starting material and (ii) enhanced charge separation efficiency. The heterostructures possess enhanced activity for the photoreduction of Ni²⁺ in water into Ni, while a benchmark TiO₂ photocatalyst was inactive. Numerous 1D and 2D titanate compounds can be easily synthesized like K₂Ti₄O₉. Therefore, this chemically exploitable weakness in the titanate edges can be used to design a variety of different heterostructured photocatalysts for the safe capture and disposal of toxic metal cations and recovery of valuable metals from the environment.

EXPERIMENTAL SECTION

Synthesis of Hyd-K₂Ti₄O₉. A 40 wt % aqueous solution of TPA was purchased from Tokyo Chemical Industry and used as received. TPA (0.78 g), NH₄F (0.014 g), and K₂Ti₄O₉ (0.2 g) were added in a Teflon-lined stainless steel autoclave, and the mixture was heated at 170 °C for 1 week. After the hydrothermal reaction, the product was washed with ethanol and dried at 60 °C.

Materials Characterization. XRD patterns of all samples were examined using a Smart Lab, RIGAKU. The UV–vis spectra of the samples were measured using a JASCO V-570UV-vis spectrophotometer. The morphology and structure of all samples were observed via FE-SEM (JEOL JEM-6500F) and (high-resolution) TEM (JEOL JEM 2100F). XPS was performed with a JEOL JPS-9010 instrument. All binding energies were calibrated in relation to the C 1s line from adventitious carbon (285 eV). Nitrogen and methanol vapor adsorption/desorption isotherms were recorded using a MicrotrakBel Belmax. The sample powders were evacuated at 120 °C for 3 h before the measurements.

Ni²⁺ Adsorption and Reduction. The sample (15 mg) was dispersed in a mixed solution of an aqueous NiCl₂·6H₂O (213 mg/L, 5 mL) solution and methanol (5 mL) in a Pyrex glass tube (34 mL), and then deaerated by Ar bubbling. The glass tube was sealed with a rubber septum and irradiated by a solar simulator (San-Ei Electric, $\lambda > 300$ nm, 1000 Wm⁻²) under stirring. After separation of the mixture, the amount of Ni²⁺ in the supernatant was measured with inductively coupled plasma atomic emission spectroscopy ICP-AES (Agilent 710-ES). The solid was analyzed by XRD and UV–vis spectroscopy to confirm the deposition of Ni semiquantitatively. Ni²⁺ adsorption was carried out without the photoirradiation. The amount of Ni²⁺ in the supernatant decreased while no Ni deposition was detected (and the color of the solid was light green, not but gray as seen in Figure 2c).

Quantitative Analysis of O₂⁻. The O₂⁻ yield of the photocatalysts was quantified according to the previous report.^{20,29} The sample (15 mg) was dispersed in an aqueous 2-propanol solution (5 mL, 4 vol %, O₂ saturated), to which nitroblue tetrazolium (NBT) had been added at a concentration of 1 mM by ultrasonication. The suspension was irradiated using a solar simulator ($\lambda > 300$ nm, 1000 Wm⁻²) for 15 min. This reaction was conducted in a Pyrex glass tube. After the irradiation, the solid was removed by centrifugation, and the supernatant was analyzed by UV–vis spectroscopy. NBT reacts with O₂⁻, generated by a reaction between O₂ and photoexcited electrons of a photocatalyst, at the molar ratio of 1:4 to form insoluble

Formazan deposits on the photocatalyst. Therefore, by quantifying the amount of NBT removed from aqueous media, the amount of generated O₂⁻ can be quantified.

Methanol Oxidation. The sample (15 mg) was dispersed in water (5 mL) containing 5 vol % of methanol in a Pyrex glass tube (34 mL), and then aerated by O₂ bubbling. The glass tube was sealed with a rubber septum and irradiated by a solar simulator under stirring. The headspace CO₂ was quantified by a Shimadzu GC-2010 plus gas chromatograph equipped with a BID detector.

H₂ Evolution. The sample (15 mg) was dispersed in water (5 mL) containing 5 vol % of methanol in a Pyrex glass tube (34 mL), and then deaerated by Ar bubbling. The glass tube was sealed with a rubber septum and irradiated by a 150 W Xe lamp with a long-pass filter (>450 nm). The headspace H₂ was quantified by a Shimadzu GC-8A gas chromatograph equipped with a TCD detector. For the apparent quantum yield (AQY) calculation, the glass tube was irradiated with a monochromated light for 3 h using a 500 W Xe lamp (Ushio) and an SM-25 monochromator (Bunkoukeiki). The number of incident photons was determined using an S1337-1010BQ silicon photodiode (Bunkoukeiki). AQY was defined by the following equation: AQY (%) = [number of evolved H₂ molecules × 2]/[number of incident photons] × 100.

ASSOCIATED CONTENT

Supporting Information

The Supporting Information is available free of charge on the ACS Publications website at DOI: 10.1021/acs.inorgchem.8b00538.

HRTEM and HADDF-STEM images, EDX elemental maps of Hyd-K₂Ti₄O₉ and Ni-deposited Hyd-K₂Ti₄O₉, XPS spectra of Ni-deposited Hyd-K₂Ti₄O₉ and P25, UV–vis spectra of P25 and NiO-grafted P25 (PDF)

AUTHOR INFORMATION

Corresponding Author

*E-mail: IDE.Yusuke@nims.go.jp.

ORCID

Yusuke Ide: 0000-0002-6901-6954

Joel Henzie: 0000-0002-9190-2645

Author Contributions

The manuscript was written through contributions of all authors.

Notes

The authors declare no competing financial interest.

ACKNOWLEDGMENTS

This work was partly supported by JSPS KAKENHI Grant Number 26708027. We thank Shinpei Enomoto (Waseda University) for TEM observation.

REFERENCES

- (1) Komarneni, S.; Kozai, N.; Paulus, W. J. Superselective Clay for Radium Uptake. *Nature* **2001**, *410*, 771–772.
- (2) Prairie, M. R.; Evans, L. R.; Stange, B. M.; Martinez, S. L. An Investigation of Titanium Dioxide Photocatalysis for the Treatment of Water Contaminated with Metals and Organic Chemicals. *Environ. Sci. Technol.* **1993**, *27*, 1776–1782.
- (3) Morishita, S.; Suzuki, K. Photoelectrochemical Deposition of Nickel onto TiO₂ Particles. Formation of Nickel Patterns without Resists. *Bull. Chem. Soc. Jpn.* **1994**, *67*, 843–846.
- (4) Forouzan, F.; Richards, T. C.; Bard, A. J. Photoinduced Reaction at TiO₂ Particles. Photodeposition from Ni^{II} Solutions with Oxalate. *J. Phys. Chem.* **1996**, *100*, 18123–18127.

- (5) Lin, W.-Y.; Rajeshwar, K. Photocatalytic Removal of Nickel from Aqueous Solutions Using UV-Irradiated TiO₂. *J. Electrochem. Soc.* **1997**, *144*, 2751–2756.
- (6) Tang, C.; Li, J.; Bando, Y.; Zhi, C.; Golberg, D. Improved TiO₂ Photocatalytic Reduction by Intrinsic Electrostatic Potential of BN Nanotubes. *Chem. - Asian J.* **2010**, *5*, 1220–1224.
- (7) Okada, T.; Ide, Y.; Ogawa, M. Organic-Inorganic Hybrids Based on Ultrathin Oxide Layers - Designed Nanostructures for Molecular Recognition. *Chem. - Asian J.* **2012**, *7*, 1980–1992.
- (8) Ide, Y.; Ochi, N.; Ogawa, M. Effective and Selective Adsorption of Zn²⁺ on a Layered Silicate from Seawater. *Angew. Chem., Int. Ed.* **2011**, *50*, 654–656.
- (9) Komatsu, Y.; Fujiki, Y. Adsorption of Cesium from Aqueous Solutions Using a Crystalline Hydrated Titanium Dioxide Fibers. *Chem. Lett.* **1980**, *9*, 1525–1528.
- (10) Sasaki, T.; Watanabe, M.; Komatsu, Y.; Fujiki, Y. Layered Hydrated Titanium Dioxide: Potassium Ion Exchange and Structural Characterization. *Inorg. Chem.* **1985**, *24*, 2265–2271.
- (11) Komatsu, Y.; Fujiki, Y.; Sasaki, T. Ion-Exchange Separation of Barium Ions and Other Alkaline Earth Metal Ions by Dihydrogen Tetratitanate Hydrate Fibers at 298 K. *Anal. Sci.* **1991**, *7*, 153–156.
- (12) Ishikawa, Y.; Tsukimoto, S.; Nakayama, K. S.; Asao, N. Ultrafine Sodium Titanate Nanowires with Extraordinary Sr Ion-Exchange Properties. *Nano Lett.* **2015**, *15*, 2980–2984.
- (13) Kudo, A.; Tanaka, A.; Domen, K.; Maruya, K.; Aika, K.; Onishi, T. Photocatalytic Decomposition of Water over NiO–K₄Nb₆O₁₇ Catalyst. *J. Catal.* **1988**, *111*, 67–76.
- (14) Youngblood, W. J.; Lee, S.-H. A.; Maeda, K.; Mallouk, T. E. Visible Light Water Splitting Using Dye-Sensitized Oxide Semiconductors. *Acc. Chem. Res.* **2009**, *42*, 1966–1973.
- (15) Gunjekar, J. L.; Kim, I. Y.; Lee, J. M.; Jo, Y. K.; Hwang, S.-J. Exploration of Nanostructured Functional Materials Based on Hybridization of Inorganic 2D Nanosheets. *J. Phys. Chem. C* **2014**, *118*, 3847–3863.
- (16) Ide, Y.; Sadakane, M.; Sano, T.; Ogawa, M. Functionalization of Layered Titanates. *J. Nanosci. Nanotechnol.* **2014**, *14*, 2135–2147.
- (17) Allen, M. R.; Thibert, A.; Sabio, E. M.; Browning, N. D.; Larsen, D. S.; Osterloh, F. E. Evolution of Physical and Photocatalytic Properties in the Layered Titanates A₂Ti₂O₉ (A = K, H) and in Nanosheets Derived by Chemical Exfoliation. *Chem. Mater.* **2010**, *22*, 1220–1228.
- (18) Xiong, Z.; Zhao, X. S. Nitrogen-Doped Titanate-Anatase Core–Shell Nanobelts with Exposed {101} Anatase Facets and Enhanced Visible Light Photocatalytic Activity. *J. Am. Chem. Soc.* **2012**, *134*, 5754–5757.
- (19) Xiong, Z.; Zhao, X. S. Titanate@TiO₂ Core–Shell Nanobelts with an Enhanced Photocatalytic Activity. *J. Mater. Chem. A* **2013**, *1*, 7738–7744.
- (20) Saito, K.; Kozeni, M.; Sohmiya, M.; Komaguchi, K.; Ogawa, M.; Sugahara, Y.; Ide, Y. Unprecedentedly Enhanced Solar Photocatalytic Activity of a Layered Titanate Simply Integrated with TiO₂ Nanoparticles. *Phys. Chem. Chem. Phys.* **2016**, *18*, 30920–30925.
- (21) Saito, K.; Tominaka, S.; Yoshihara, S.; Ohara, K.; Sugahara, Y.; Ide, Y. Room-Temperature Rutile TiO₂ Nanoparticle Formation on Protonated Layered Titanate for High-Performance Heterojunction Creation. *ACS Appl. Mater. Interfaces* **2017**, *9*, 24538–24544.
- (22) Zhang, P.; Yokoyama, T.; Itabashi, O.; Wakui, Y.; Suzuki, T. M.; Inoue, K. Recovery of Metal Values from Spent Nickel-Metal Hydride Rechargeable Batteries. *J. Power Sources* **1999**, *77*, 116–122.
- (23) Honda, K.; Ide, Y.; Tsunoji, N.; Torii, M.; Sadakane, M.; Sano, T. An Efficient Way to Synthesize Hiroshima University Silicate-1 (HUS-1) and the Selective Adsorption Property of Ni²⁺ from Seawater. *Bull. Chem. Soc. Jpn.* **2014**, *87*, 160–166.
- (24) Ide, Y.; Inami, N.; Hattori, H.; Saito, K.; Sohmiya, M.; Tsunoji, N.; Komaguchi, K.; Sano, T.; Bando, Y.; Golberg, D.; Sugahara, Y. Remarkable Charge Separation and Photocatalytic Efficiency Enhancement through Interconnection of TiO₂ Nanoparticles by Hydrothermal Treatment. *Angew. Chem., Int. Ed.* **2016**, *55*, 3600–3605.
- (25) Hattori, H.; Ide, Y.; Sano, T. Microporous Titanate Nanofibers for Highly Efficient UV-Protective Transparent Coating. *J. Mater. Chem. A* **2014**, *2*, 16381–16388.
- (26) Ide, Y.; Shirae, W. Hydrothermal Conversion of Layered Niobate K₄Nb₆O₁₇·3H₂O to Rare Microporous Niobate K₆Nb_{10.8}O₃₀. *Inorg. Chem.* **2017**, *56*, 10848–10851.
- (27) Easteal, A. J.; Udy, D. J. Preparation and Properties of Potassium Titanates. *High Temp. Sci.* **1972**, *4*, 487–495.
- (28) Ohtani, B.; Okugawa, Y.; Nishimoto, S.; Kagiya, T. Photocatalytic Activity of Titania Powders Suspended in Aqueous Silver Nitrate Solution: Correlation with pH-Dependent Surface Structures. *J. Phys. Chem.* **1987**, *91*, 3550–3555.
- (29) Goto, H.; Hanada, Y.; Ohno, T.; Matsumura, M. Quantitative Analysis of Superoxide Ion and Hydrogen Peroxide Produced from Molecular Oxygen on Photoirradiated TiO₂ Particles. *J. Catal.* **2004**, *225*, 223–229.
- (30) Ide, Y.; Matsuoka, M.; Ogawa, M. Efficient Visible-Light-Induced Photocatalytic Activity on Gold-Nanoparticle-Supported Layered Titanate. *J. Am. Chem. Soc.* **2010**, *132*, 16762–16764.
- (31) Doustkhah, E.; Rostamnia, S.; Tsunoji, N.; Henzie, J.; Takei, T.; Yamauchi, Y.; Ide, Y. Templated Synthesis of Atomically-Thin Ag Nanocrystal Catalysts in the Interstitial Space of a Layered Silicate. *Chem. Commun.* **2018**, *54*, 4402–4405.
- (32) Kirumakki, S. R.; Shpeizer, B. G.; Sagar, G. V.; Chary, K. V. R.; Clearfield, A. *J. Catal.* **2006**, *242*, 319–331.
- (33) Tada, S.; Kikuchi, R.; Wada, K.; Osada, K.; Akiyama, K.; Satokawa, S.; Kawashima, Y. *J. Power Sources* **2014**, *264*, 59–66.
- (34) Prieto-Mahaney, O.-O.; Murakami, N.; Abe, R.; Ohtani, B. Correlation between Photocatalytic Activities and Structural and Physical Properties of Titanium(IV) Oxide Powders. *Chem. Lett.* **2009**, *38*, 238–239.
- (35) Ide, Y.; Komaguchi, K. A Photocatalytically Inactive Microporous Titanate Nanofiber as an Excellent and Versatile Additive to Enhance the TiO₂ Photocatalytic Activity. *J. Mater. Chem. A* **2015**, *3*, 2541–2546.
- (36) Jin, Q.; Ikeda, T.; Fujishima, M.; Tada, H. Nickel(II) Oxide Surface-Modified Titanium(IV) Dioxide as a Visible-Light-Active Photocatalyst. *Chem. Commun.* **2011**, *47*, 8814–8816.
- (37) Ide, Y.; Kawamoto, N.; Bando, Y.; Hattori, H.; Sadakane, M.; Sano, T. Ternary Modified TiO₂ as Simple and Efficient Photocatalyst for Green Organic Synthesis. *Chem. Commun.* **2013**, *49*, 3652–3654.
- (38) Murakami, N.; Chiyoya, T.; Tsubota, T.; Ohno, T. Switching Redox Site of Photocatalytic Reaction on Titanium(IV) Oxide Particles Modified with Transition-Metal Ion Controlled by Irradiation Wavelength. *Appl. Catal., A* **2008**, *348*, 148–152.